



Synchrotron X-ray microbeam dosimetry with a 20 micrometre resolution scintillator fibre-optic dosimeter

James Archer,^a Enbang Li,^{a*} Marco Petasecca,^{a,b} Andrew Stevenson,^c Jayde Livingstone,^c Andrew Dipuglia,^a Jeremy Davis,^{a,b} Anatoly Rosenfeld^{a,b} and Michael Lerch^{a,b}

Received 9 December 2017

Accepted 20 February 2018

Edited by S. M. Heald, Argonne National Laboratory, USA

Keywords: microbeam radiation therapy; scintillator dosimetry; fibre-optic dosimeters.

^aCentre for Medical Radiation Physics, University of Wollongong, Wollongong, NSW 2522, Australia,

^bIllawarra Health and Medical Research Institute, University of Wollongong, NSW 2522, Australia, and

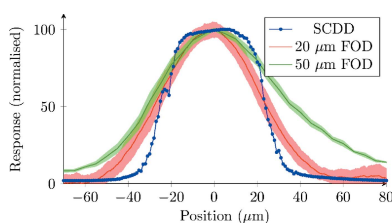
^cImaging and Medical Beam-Line, Australian Synchrotron, Clayton, VIC 3168, Australia.

*Correspondence e-mail: enbang@uow.edu.au

Cancer is one of the leading causes of death worldwide. External beam radiation therapy is one of the most important modalities for the treatment of cancers. Synchrotron microbeam radiation therapy (MRT) is a novel pre-clinical therapy that uses highly spatially fractionated X-ray beams to target tumours, allowing doses much higher than conventional radiotherapies to be delivered. A dosimeter with a high spatial resolution is required to provide the appropriate quality assurance for MRT. This work presents a plastic scintillator fibre optic dosimeter with a one-dimensional spatial resolution of 20 μm , an improvement on the dosimeter with a resolution of 50 μm that was demonstrated in previous work. The ability of this probe to resolve microbeams of width 50 μm has been demonstrated. The major limitations of this method were identified, most notably the low-light signal resulting from the small sensitive volume, which made valley dose measurements very challenging. A titanium-based reflective paint was used as a coating on the probe to improve the light collection, but a possible effect of the high-Z material on the probes water-equivalence has been identified. The effect of the reflective paint was a $28.5 \pm 4.6\%$ increase in the total light collected; it did not affect the shape of the depth-dose profile, nor did it explain an over-response observed when used to probe at low depths, when compared with an ionization chamber. With improvements to the data acquisition, this probe design has the potential to provide a water-equivalent, inexpensive dosimetry tool for MRT.

1. Introduction

Synchrotron microbeam radiation therapy (MRT) is a pre-clinical external beam therapy that uses highly collimated, high fluence X-rays that are spatially fractionated into multiple microbeams. The X-rays used in this work are fractionated into arrays of 50 μm microbeams with a spacing (peak-to-peak) of 400 μm (from the Australian Synchrotron, which is a common but not exclusive configuration for MRT), and have an average energy of 94.4 keV, with the energy tail extending beyond 200 keV (Stevenson *et al.*, 2017; Crosbie *et al.*, 2013). In a number of cell and animal studies, healthy tissue has been shown to be resilient to MRT unlike tumour tissue, which is susceptible to high doses (Bouchet *et al.*, 2012, 2016; Anderson *et al.*, 2014; Bronnimann *et al.*, 2016). It has been hypothesized that this sparing of healthy tissue can allow patients with malignant central nervous system tumours, who currently have no safe therapies available to them, to be



© 2018 International Union of Crystallography

treated with MRT (Bravin *et al.*, 2015; Grotzer *et al.*, 2015). The high dose rate of MRT allows the required quantity to be delivered to the target quickly and with minimal dose blurring.

This high dose rate and fine spatial structure of the microbeams makes MRT dosimetry a challenging area. Ionization chambers, the ‘gold standard’ of dosimetry, are able to handle the high dose rates, with some calibration challenges (Fournier, Crosbie *et al.*, 2016), but cannot achieve the resolution required to measure the peak-to-valley dose ratio (PVDR). Radiochromic film can measure individual microbeams, but granularity limits the resolution of the film. The film also lacks the range to measure both peak and valley dose on the same exposure, cannot provide real-time dosimetry, and can be inaccurate by up to 15% (Bartzsch *et al.*, 2015). Metal oxide semiconductor field-effect transistors (MOSFET) have sub-micrometre spatial resolution and a low aspect ratio so are very successful for measuring microbeams. However, MOSFETs suffer radiation damage because of the high dose rate and hence have a short lifespan (Rosenfeld *et al.*, 1999, 2001). Silicon strip detectors (SSDs) can be manufactured with high enough spatial resolutions to resolve microbeams (Petasecca *et al.*, 2012; Fournier, Cornelius *et al.*, 2016; Fournier *et al.*, 2017; Davis *et al.*, 2018). Single-crystal diamond detectors (SCDDs) have the greatest one-dimensional spatial resolution (1 μm) and have been very successful in microbeam measurements (Livingstone *et al.*, 2016). Alignment remains a time-consuming step in the setup of SCDD, as small misalignments can result in a large reduction in the spatial resolution due to the large aspect ratio of the dosimeter (a cylindrical sensitive volume of 2 mm diameter and 1 μm thickness). This is also a challenge for SSD devices. Three-dimensional dosimetry can be performed with PRESAGE, a radiochromic polyurethane-based dosimeter. PRESAGE itself has a very high resolution, able to capture three-dimensional information on complex microbeam treatments using overlapping dose deliveries. The challenge associated with using PRESAGE is measuring this information. Optical computed tomography (McErlean *et al.*, 2016) and confocal microscopy (Gagliardi *et al.*, 2015) are able to measure the spatial information with high precision (approximately 20 μm with optical computed tomography and less than 1 μm with confocal microscopy). However, measuring dose information is currently not possible, and cannot provide real-time results.

We are investigating scintillator fibre-optic dosimeters (FODs) as they have desirable properties that other dosimeters lack. Primarily, the plastic scintillator used is water equivalent (Beddar *et al.*, 1992a), meaning the dose measured by the probe is the dose of clinical interest. Plastic scintillators also boast temperature independence over experimental and clinical ranges, linearity with total absorbed dose, energy independence (Beddar *et al.*, 1992a,b), in addition to being relatively easy and inexpensive to manufacture from the base components. The spatial resolution of scintillator FODs is determined by the thickness of the scintillator used on the end of the fibre optic. Dosimeters using a plastic scintillator have been applied to a number of radiation therapies, such as high-

energy photon-beam therapy (Archer *et al.*, 2017a; Kim *et al.*, 2013), brachytherapy (Sliski *et al.*, 2005) and prostate cancer therapy (Klawikowski *et al.*, 2014).

We have demonstrated the ability of a plastic scintillator FOD to resolve microbeams and measure depth-dose profiles in recent work (Archer *et al.*, 2017b). We had achieved an ‘ideal’ (ideal in this context meaning the best resolution achievable by this probe, given optimal alignment with respect to the beam) one-dimensional spatial resolution of 50 μm . We now present a dosimeter with an improved spatial resolution of 20 μm .

A major advantage of FOD probes is the relatively inexpensive materials used. The fabrication of the probe can be carried out by hand, with the scintillator polished down to the desired thickness (currently a metal template of pre-determined thickness is used to determine the scintillator thickness and prevent over-polishing) and then optically coupled to the fibre. As such, the important qualities of the probe can be easily altered during fabrication. The light collected can be increased by using a large core fibre, at the expense of misalignment sensitivity. The spatial resolution can be improved by polishing the scintillator to a thinner layer, at the expense of sensitivity. Different scintillator materials can be used to increase spectrum overlap between the scintillator light and photomultiplier sensitivity spectra. Thus, using FODs allows for variations to be introduced with ease during fabrication, an advantage most other dosimeters lack. The goal of this project is to develop FODs into a system that can quickly and reliably measure the PVDR and microbeam structures in MRT fields. With the use of an appropriate calibration source, we also anticipate the application of this system in absolute dosimetry. This work is the next step in this project; to improve the resolution of the probe and investigate the effects that arise from using a decreased sensitive volume.

2. Materials and methods

The dosimetry probe used here is an improvement on the probe design used in previous experimental work (Archer *et al.*, 2017b). The BC-400 plastic scintillator is optically coupled to an Eska CK-40 plastic optical fibre. The scintillator is fashioned into a cylindrical section, with a length of 20 μm and a diameter of 2 mm. The core of the fibre is 1 mm in diameter (with cladding and shielding making the total diameter 2 mm), hence the effective area in which light can be collected is 1 mm in diameter. This gives a sensitive volume of 0.0157 mm³ and an ideal one-dimensional spatial resolution of 20 μm , an improvement on the previously reported resolution of 50 μm . The probe is illustrated in Fig. 1.

To improve the light signal strength, the probe is coated in a layer of BC-620 reflective paint a few hundred micrometres thick. The paint reflects more light into the acceptance cone of the optical fibre. However, as the paint is composed of TiO₂ (40% by mass), the higher-Z titanium atoms could result in dose enhancement, which compromises the water equivalence of the probe. This could also cause an increase in the light produced, which, while increasing the signal, is not the water

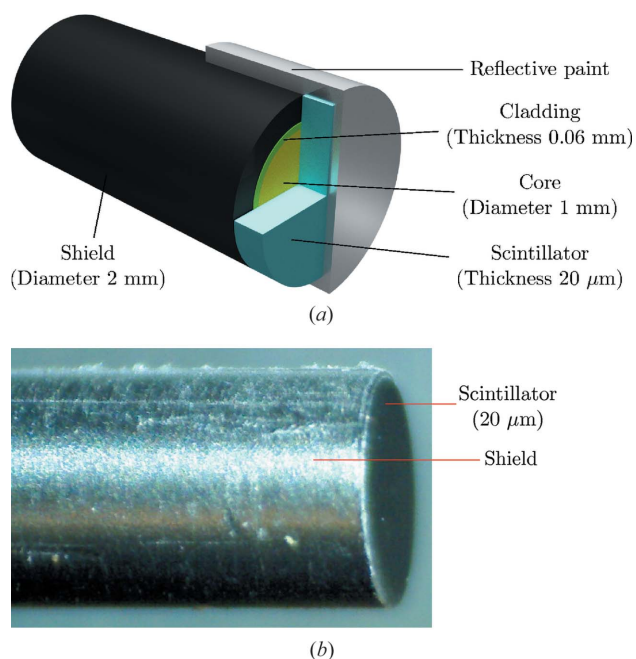


Figure 1
 (a) A polished scintillator coupled to large core fibre (not to scale). (b) A microscope image of the probe tip, without the reflective paint. The scintillator is the dark thin layer on the end. For maximum one-dimensional resolution, the radiation beam must be incident perpendicular to the fibre axis.

equivalent dose and so is undesirable. We will investigate the effects of the BC-620 reflective paint in this work.

The light signal was measured by a SensL MiniSM Silicon Photomultiplier 10035 (SiPM). This signal was digitized with a Texas Instruments 14-bit Analogue Front End (AFE). The digital signal readout was produced using customized in-house software, which allowed the signal to be integrated over any sampling duration at a given frequency.

The experiment was performed on the Imaging and Medical Beam-Line (IMBL) at the Australian Synchrotron, illustrated in Fig. 2. The IMBL hosts *in vitro* and *in vivo* MRT studies, and potentially human studies in the future (Pelliccia *et al.*, 2016; Livingstone *et al.*, 2017; Poole *et al.*, 2017). The synchrotron was operated with the standard 200 mA beam current. The IMBL configuration was 3.0 T wiggler field, with filter set F4

(Stevenson *et al.*, 2017) which defines the beam intensity and energy spectrum. The X-rays are spatially fractionated into microbeams using a tungsten carbide multi-slit collimator (MSC) with 50 µm spacing and 400 µm pitch. The size of the beam at the probe is determined by a beam-defining aperture (BDA). The available BDAs have width 30 mm and heights of 2.014, 1.052 and 0.532 mm. For this work, the 2.014 mm BDA was used to increase the total photon fluence into the probe for the maximum light signal. All results presented in this paper were performed in a water tank, with a Kapton tape entrance window; this provided the appropriate backscatter and allowed the probe to be easily mounted and moved in depth. The details of this water tank are described by Livingstone *et al.* (2017).

Two experiments were performed, one to measure the intrinsic microbeam profile and the other to measure the effect of the BC-620 reflective paint on the probe. The microbeam scan was performed with the probe mounted in edge-on mode, along the *y* direction (the coordinate system used for measurements is defined in Fig. 2). This allowed the probe to use the maximum one-dimensional spatial resolution of 20 µm. The probe was scanned over a distance of 30 mm at a speed of 0.1 mm s⁻¹. The SiPM was integrated over a time of 200 µs at a frequency of 1 kHz. For comparison, a microbeam was scanned in 1 µm steps by a PTW microDiamond SCDD at the same depth and with the same BDA. The microDiamond has a 0.004 mm³ sensitive volume with an ideal spatial resolution of 1 µm. The microDiamond was scanned vertically through the field (in the *z* direction) at each 1 µm step (in the *y* direction), and the total response was integrated using a PTW UNIDOS electrometer. While this is different to how the FOD data were measured, the profile shape averaged over the *z* direction is suitable to illustrate how volume averaging affects the measured microbeam shapes.

The effects of the paint were quantified by measuring a depth-dose profile with and without the paint. This was compared with a PinPoint N31014 ionization chamber (IC), with a sensitive volume of 0.015 cm³. The sensitive volume of the IC is too large to resolve microbeams, therefore, in order to compare dosimetry devices, the probes are scanned through broadbeam fields (without the MSC in place). To compare the IC and FOD appropriately, the probes were scanned vertically

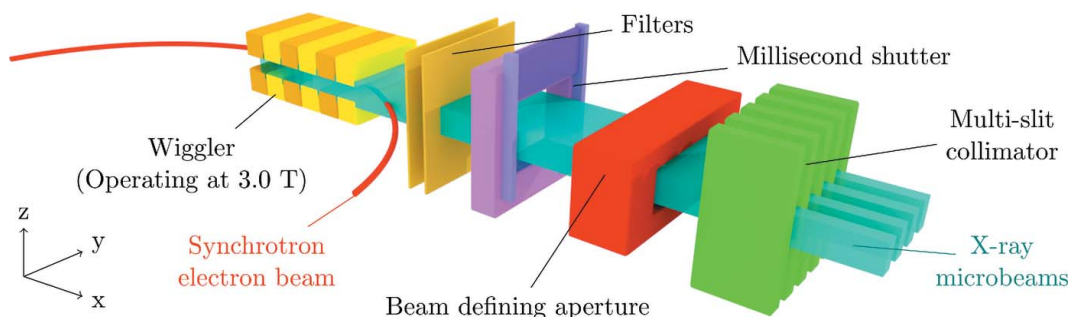


Figure 2
 Diagram of the Australian Synchrotron Imaging and Medical Beam-Line components that are relevant to this work. The coordinate system used defines the beam direction as *x*, with microbeams fractionated in the *y* direction, and height in the *z* direction.

(z) through the centre of the broadbeam X-ray field, and the net response above background was integrated. The IC has been calibrated by PTW with a TH 200 (109 keV mean energy) X-ray beam, hence the accumulated charge can be converted to total dose in water. The IC response is energy independent in the experimental ranges used here. For the FOD, the total SiPM charge throughout the scan (in 500 μ s and 500 Hz sampling intervals) was measured. This was carried out between 15 and 100 mm for both the IC and the FOD with and without reflective paint. The measurement was repeated three times at each depth to evaluate the repeatability of the result.

In both experiments, the background light signal must be subtracted from the raw measurement from the FOD. An average response is measured outside the field and subtracted from all values. As the signal is very noisy with such a small sensitive volume, the fluctuations will go below zero after the average background is removed. Furthermore, there will be Cherenkov and fluorescence light generated throughout the scintillator and fibre optic (Čerenkov, 1937). Although the threshold for Cherenkov radiation in this plastic system is 175 keV photons (Archer *et al.*, 2017c), there is still a small effect observed in these probes in synchrotron X-ray beams because the IMBL X-ray spectra have some components above 175 keV, which can compromise the spatial resolution. Since the total Cherenkov and fluorescence contribution to the signal will be proportional to the length of fibre optic exposed to the radiation field, a linear fit to the total response when the scintillator is out of the field on either side will allow this contribution to be calculated and subtracted. This was achieved by detecting the first and last microbeam, and using these points in the data to determine the out-of-field response on both sides of the microbeam profile. Using the difference between the out-of-field responses, the Cherenkov and fluorescence gradient was found and then used to generate a ramp function between the two edges defined by the outer microbeams. The ramp function was used to generate values that can be subtracted from each point within the regions affected by Cherenkov and fluorescence. This was carried out for the microbeam scan but not for the depth-dose experiment as the spatial resolution is not being exploited.

The paint was applied by immersing the probe in a container of the paint. Once this had dried, a layer of oil-based enamel paint was applied by a similar process to the surface in order to prevent the water-soluble BC-620 dissolving in the water tank. This increased the diameter of the probe by up to several tenths of a millimetre, and the uniformity of application could not be guaranteed.

3. Results and discussion

3.1. Improvement of the spatial resolution

The scan of the intrinsic microbeam field is shown in Fig. 3. The data were smoothed using an unweighted moving average with a width of 200 samples, corresponding to a distance of 20 μ m [the method of unweighted moving average is described

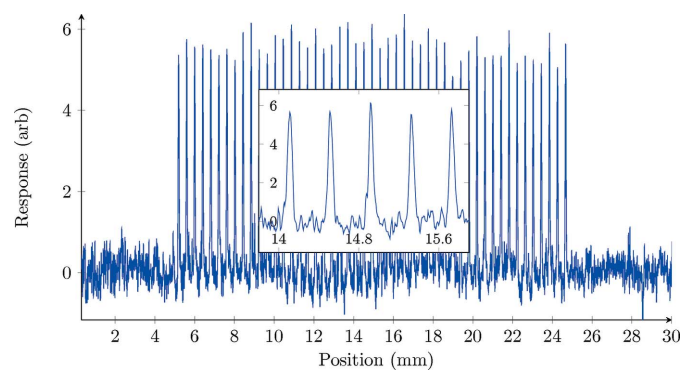


Figure 3

The intrinsic microbeam profile measured using FOD, scanning at 0.1 mm s⁻¹. The background and Cherenkov subtraction has been performed, as well as the unweighted moving average smoothing with a window of 200 points. The inset shows the central five microbeams.

by Archer *et al.* (2017c) as ‘boxcar smoothing’]. The average FWHM for individual microbeams in the scan was $52.1 \pm 6.5 \mu\text{m}$, which is in good agreement with the microDiamond SCDD measurements $49.5 \pm 1.4 \mu\text{m}$, and a significant improvement over previous results ($63 \pm 2 \mu\text{m}$) for the 50 μm FOD. It is important to note that the 50 μm probe used Gammex RMI457 Solid Water instead of water as the scattering material, but earlier work has demonstrated that there is no more than a 6% difference in dose deposited in these materials under identical MRT irradiation (Cameron *et al.*, 2017). The measured FWHM is indicative of the spatial resolution of the probe. As the scintillator thickness approaches zero, the measured FWHM approaches the true value. The results have demonstrated an improvement in resolution from the 50 μm probe to the 20 μm probe. However, as the sensitive volume is made smaller, the amount of light created will decrease. As such, there is an optimal thickness whereby the measured FWHM will be equal to the true value (within uncertainties) while maximizing the light generated.

In ideal conditions, without beam divergence or scattering, the microbeam shapes would appear much more rectangular, with a sharper penumbra. As shown in Fig. 4, microbeams measured with the microDiamond SCDD (which, due to a high spatial resolution of 1 μm , gives a very accurate microbeam shape) have a flat top and edges that rise more sharply, whereas the microbeams measured with the FOD are

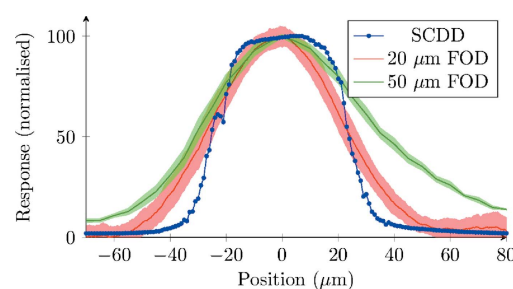


Figure 4

Individual microbeam shape comparison between the 20 μm FOD, the 50 μm FOD (Archer *et al.*, 2017b) and microDiamond SCDD. The average of the microbeams measured with the FOD and the standard deviation are shown.

quite triangular in shape. Also shown is the average of a number of microbeams measured using the 50 μm probe from Archer *et al.* (2017b). The shape arises from volume averaging across the probe, which is reduced for smaller sensitive volumes. We can see from this figure that the asymmetry observed in the right side of the 50 μm microbeam measurement is significantly less for the 20 μm results.

Much like the SCDD devices, the large diameter of the scintillator compared with the thickness makes alignment very important for this probe. A misalignment causes an increase in the size of the cross section exposed to the beam proportional to the angle of misalignment and the diameter of the probe (for small angles). Therefore, a misalignment can increase the measured FWHM, and so alignment of the probe is important for accurate dosimetry.

The measured FWHM is consistent with the reduced sensitive volume, assuming the alignment was optimal. However, it is possible that the spatial resolution was greater than 20 μm , and the probe was also misaligned to produce this result. Therefore, an independent method is required to verify the thickness of the probes and we intend to use microscopy for this purpose in future probe fabrications.

The decreased sensitive volume has made the signal-to-noise ratio quite low. The error in the average FWHM measured using this probe is larger than the error associated with the 50 μm probe (6.5 μm compared with 2 μm). The noise in the profile has been reduced with smoothing, but a smoothing window greater than 200 samples caused the heights of the microbeams to decrease because of this additional artificial volume-averaging effect. As a result of the poor valley signal, we were unable to even attempt calculation of PVDR for these results as the uncertainty will be many times greater than the PVDR value itself. Despite this, it appears that the valley dose is much closer to zero than with the 50 μm probe, suggesting that with improvements to light collection techniques it may be possible to measure a more accurate PVDR than with the 50 μm probe.

3.2. Effect of reflective paint

The depth-dose curve is presented in Fig. 5(a), with the normalized results compared to IC shown in Fig. 5(b). Application of the reflective paint to the probe end increased the average light collected by $28.5 \pm 4.6\%$. The over-response present in previous data is still evident in this result. The FOD and IC data match very well at greater depths, suggesting that the FOD results are over-responding even at a depth of 20 mm (the depth at which normalization is the standard). As shown in Fig. 5(b), the shape of the depth-dose curve was not affected by the paint, and so the discrepancy between the IC and FOD at low depths cannot be explained by the use of the non-water-equivalent paint, and so remains an open question. In Fig. 5(c), the percentage difference between the FOD response and the IC response has been calculated. This shows more clearly that the main difference is at depths lower than 40 mm, with the discrepancy being less for the probe without paint at greater depths. The IC has been validated for depths

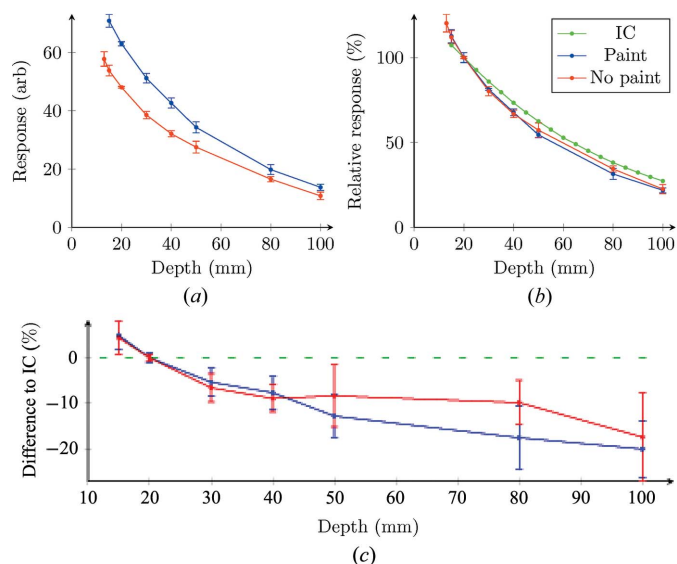


Figure 5 Percentage depth dose measured with and without the BC-620 reflective paint. (a) The direct comparison between the light output, as measured under both conditions. The scale is the integrated signal output, which is arbitrary but comparable for similarly collected data. (b) Both responses normalized to 20 mm depth and compared with a PinPoint N31014 ionization chamber. (c) The percentage difference between the two sets of FOD data. Error bars shown are the 95% confidence intervals from the three measurements at each depth. The error bars on the IC data were negligible and have been omitted.

greater than 20 mm in water. As the beam height is nearly the same size as the IC diameter, this means that, despite the IC being the dosimetry standard, the IC is limited in its application to small-field dosimetry, and so a direct comparison between the FOD and IC at less than 20 mm depth may not be valid. We plan on fabricating probes with similar sensitive volumes to the IC (2 mm diameter, 5 mm length) in order to investigate whether the effect is the result of volume averaging. Possible non-linear dose responses and dose enhancement effects of the BC-620 paint will also be investigated in a future Monte Carlo study.

3.3. Signal strength

These results indicate that the main challenge associated with performing dosimetry with this probe is the low sensitivity. Smaller sensitive volumes are necessary for enhanced spatial resolution, hence improvements in light-collection techniques are required in order to optimize the signal-to-noise ratio. One of the most significant limitations in light collection is the use of the AFE device to digitize the signal. The AFE collects current over an integration period to measure the total charge accumulation, and there is a total charge limit on the device, above which saturation occurs. This limits the total integration time of the device. Furthermore, the SiPM raw current is converted to a voltage *via* an internal transimpedance amplifier, which is then converted back to current at the AFE connection, having the potential to introduce more noise into the signal. We are currently investigating the use of a 500 MHz 5 GS s^{-1} oscilloscope to

measure the SiPM output voltage directly, with custom-made software to integrate the signal over varied durations. This will remove the upper limit on the current imposed by the AFE, as well as provide a robust environment for implementing different algorithms in order to test the optimal procedure for signal integration (such as net light integration or single photon counting).

Alternatives to the BC-620 reflective paint are being investigated. The most promising candidate is sputtering deposition of aluminium onto the end of the probe. Aluminium has a lower atomic mass than titanium so will have a reduced effect on the water-equivalence. Furthermore, the aluminium can be applied in layers that are far less thick than the BC-620 paint (on the micrometre scale). This will have a greater effect on the light captured because the aluminium will have a more specular reflectance, whereas the BC-620 is diffuse, and so more light will be guided into the acceptance cone of the fibre. This will also decrease the effect of misalignment as less light from outside the acceptance cone will be scattered into it due to the specular nature of the reflective surface, reducing the effective diameter of the collection volume/area.

4. Conclusions

We have demonstrated a water-equivalent plastic scintillator fibre optic dosimeter with an ideal one-dimensional spatial resolution of 20 μm . This is significant as most dosimeters currently under consideration for MRT quality assurance are not water-equivalent. The probe has been used to resolve individual 50 μm microbeams. Light signal strength remains a challenge in gaining accurate relative dose values. Depth-dose data have been replicated with the higher resolution probe and the BC-620 reflective paint has no effect on the shape of the depth-dose curve. This cannot explain the over-response at lower depths when compared with an ionization chamber. Low signal in the valley regions makes calculating the PVDR impossible; improvements to the data acquisition are being investigated to overcome this limitation.

A probe with an even higher spatial resolution and smaller sensitive volume is being fabricated, with the aim of improving the spatial resolution and minimizing volume-averaging effects. As such, the improvements in data acquisition are not only vital for improving the signal-to-noise ratio in this probe but will also be necessary if a 10 μm resolution probe is to be tested. Despite the current limitations, this dosimeter probe design has a high potential to provide real-time water-equivalent MRT dosimetry at low cost.

Funding information

This project was supported by The University of Wollongong's Global Challenges Program. This research was undertaken on the Imaging and Medical Beam Line at the Australian Synchrotron, part of ANSTO (Comparison and evaluation of alternate dosimeter technologies for MRT, AS172/IMBL/12154). Authors JA, JD, AD and ML acknowledge the support

of the Australian National Health and Medical Research Council (grant No. APP1093256). This research has been conducted with the support of the Australian Government Research Training Program Scholarship.

References

- Anderson, D. L., Mirzayans, R., Andrais, B., Siegbahn, E. A., Fallone, B. G. & Warkentin, B. (2014). *J. Synchrotron Rad.* **21**, 801–810.
- Archer, J., Li, E., Petasecca, M., Dipuglia, A., Cameron, M., Stevenson, A., Hall, C., Häusermann, D., Rosenfeld, A. & Lerch, M. (2017b). *Sci. Rep.* **7**, 12450.
- Archer, J., Li, E., Petasecca, M., Lerch, M., Rosenfeld, A. & Carolan, M. (2017a). *Med. Phys.* **44**, 1965–1968.
- Archer, J., Madden, L., Li, E., Carolan, M., Petasecca, M., Metcalfe, P. & Rosenfeld, A. (2017c). *Phys. Med.* **42**, 185–188.
- Bartzsch, S., Lott, J., Welsch, K., Bräuer-Krisch, E. & Oelfke, U. (2015). *Med. Phys.* **42**, 4069–4079.
- Beddar, A. S., Mackie, T. R. & Attix, F. H. (1992a). *Phys. Med. Biol.* **37**, 1883–1900.
- Beddar, A. S., Mackie, T. R. & Attix, F. H. (1992b). *Phys. Med. Biol.* **37**, 1901–1913.
- Bouchet, A., Boumendjel, A., Khalil, E., Serduc, R., Bräuer, E., Siegbahn, E. A., Laissue, J. A. & Boutonnat, J. (2012). *J. Synchrotron Rad.* **19**, 478–482.
- Bouchet, A., Potez, M. T., Flaender, M., Schaad, L., Rome, C., Farion, R., Laissue, J. A., Grotzer, M., Djonov, V., Elleaume, H., Brun, E. & Serduc, R. (2016). *Int. J. Radiat. Oncol. Biol. Phys.* **96**, E94–E95.
- Bravin, A., Olko, P., Schültke, E. & Wilkens, J. J. (2015). *Phys. Med.* **31**, 561–563.
- Bronnimann, D., Bouchet, A., Schneider, C., Potez, M., Serduc, R., Brauer-Krisch, E., Graber, W., von Gunten, S., Laissue, J. A. & Djonov, V. (2016). *Sci. Rep.* **6**, 33601.
- Cameron, M., Cornelius, I., Cutajar, D., Davis, J., Rosenfeld, A., Lerch, M. & Guatelli, S. (2017). *J. Synchrotron Rad.* **24**, 866–876.
- Čerenkov, P. A. (1937). *Phys. Rev.* **52**, 378–379.
- Crosbie, J. C., Rogers, P. A. W., Stevenson, A. W., Hall, C. J., Lye, J. E., Nordstrom, T., Midgley, S. M. & Lewis, R. A. (2013). *Med. Phys.* **40**, 62103.
- Davis, J. A., Paino, J., Dipuglia, A., Cameron, M., Petasecca, M., Pastuovic, Z., Siegele, R., Rosenfeld, A. B., Perevertaylo, V. L. & Lerch, M. L. F. (2018). *Biomed. Phys. Eng. Express*, doi:10.1088/2057-1976/aab10c.
- Fournier, P., Cornelius, I., Dipuglia, A., Cameron, M., Davis, J. A., Cullen, A., Petasecca, M., Rosenfeld, A. B., Bräuer-Krisch, E., Häusermann, D., Stevenson, A. W., Perevertaylo, V. & Lerch, M. L. F. (2017). *Rad. Meas.* **106**, 405–411.
- Fournier, P., Cornelius, I., Donzelli, M., Requardt, H., Nemoz, C., Petasecca, M., Bräuer-Krisch, E., Rosenfeld, A. & Lerch, M. (2016). *J. Synchrotron Rad.* **23**, 1180–1190.
- Fournier, P., Crosbie, J. C., Cornelius, I., Berkvens, P., Donzelli, M., Clavel, A. H., Rosenfeld, A. B., Petasecca, M., Lerch, M. L. F. & Bräuer-Krisch, E. (2016). *Phys. Med. Biol.* **61**, N349–N361.
- Gagliardi, F. M., Cornelius, I., Blencowe, A., Franich, R. D. & Geso, M. (2015). *Med. Phys.* **42**, 6973–6986.
- Grotzer, M. A., Schültke, E., Bräuer-Krisch, E. & Laissue, J. A. (2015). *Phys. Med.* **31**, 564–567.
- Kim, K. A., Yoo, W. J., Jang, K. W., Moon, J., Han, K. T., Jeon, D., Park, J. Y., Cha, E. J. & Lee, B. (2013). *Radiat. Prot. Dosim.* **153**, 294–299.
- Klawikowski, S. J., Zeringue, C., Wootton, L. S., Ibbott, G. S. & Beddar, S. (2014). *Phys. Med. Biol.* **59**, N27–N36.
- Livingstone, J., Adam, J.-F., Crosbie, J. C., Hall, C. J., Lye, J. E., McKinlay, J., Pelliccia, D., Pouzoulet, F., Prezado, Y., Stevenson, A. W. & Häusermann, D. (2017). *J. Synchrotron Rad.* **24**, 854–865.

- Livingstone, J., Stevenson, A. W., Butler, D. J., Häusermann, D. & Adam, J.-F. (2016). *Med. Phys.* **43**, 4283–4293.
- McErlean, C. M., Bräuer-Krisch, E., Adamovics, J. & Doran, S. J. (2016). *Phys. Med. Biol.* **61**, 320–337.
- Pelliccia, D., Poole, C. M., Livingstone, J., Stevenson, A. W., Smyth, L. M. L., Rogers, P. A. W., Häusermann, D. & Crosbie, J. C. (2016). *J. Synchrotron Rad.* **23**, 566–573.
- Petasecca, M., Cullen, A., Fuduli, I., Espinoza, A., Porumb, C., Stanton, C., Aldosari, A. H., Brauer-Krisch, E., Requardt, H., Bravin, A., Perevertaylo, V., Rosenfeld, A. B. & Lerch, M. L. F. (2012). *J. Instrum.* **7**, P07022.
- Poole, C. M., Day, L. R. J., Rogers, P. A. W. & Crosbie, J. C. (2017). *Biomed. Phys. Eng. Express*, **3**, 025001.
- Rosenfeld, A., Kaplan, G., Kron, T., Allen, B., Dilmanian, A., Orion, I., Ren, B., Lerch, M. & Holmes-Siedle, A. (1999). *IEEE Trans. Nucl. Sci.* **46**, 1774–1780.
- Rosenfeld, A., Lerch, M., Kron, T., Brauer-Krisch, E., Bravin, A., Holmes-Siedle, A. & Allen, B. (2001). *IEEE Trans. Nucl. Sci.* **48**, 2061–2068.
- Sliski, A., Mitch, M. & Soares, C. (2005). *Med. Phys.* **32**, 2137.
- Stevenson, A. W., Crosbie, J. C., Hall, C. J., Häusermann, D., Livingstone, J. & Lye, J. E. (2017). *J. Synchrotron Rad.* **24**, 110–141.